Inorg. Chem. **2007**, *46*, 486–496

Ligand Structural Effects on Cu_2S_2 Bonding and Reactivity in Side-On Disulfido-Bridged Dicopper Complexes

Eric C. Brown, Itsik Bar-Nahum, John T. York, Nermeen W. Aboelella, and William B. Tolman*

Department of Chemistry and Center for Metals in Biocatalysis, University of Minnesota, 207 Pleasant Street Southeast, Minneapolis, Minnesota 55455

Received August 22, 2006

To assess supporting ligand effects on S–S bond activation, a series of $[Cu_2(\mu\text{-}\eta^2\text{:}\eta^2\text{-}S_2)]^{2+}$ complexes supported by various β-diketiminate or anilido-imine ligands (L) were synthesized via the reaction of Cu(I) precursors LCu(CH$_3$CN) with S_8. For the cases where L = β-diketiminate, the syntheses were complicated by formation of clusters $[Cu(SR)]_4$, where SR represents the ligand functionalized by sulfur at the central methine position. The $[Cu_2(\mu\text{-}\eta^2\text{:}\eta^2\text{-}S_2)]^{2+}$ products were characterized by X-ray crystallography and electronic absorption and resonance Raman spectroscopy. Correlations among the Cu–S, Cu–Cu, and S–S distances and the ν(S–S) values were observed and interpreted within the framework of a previously described bonding picture (Chen, P.; Fujisawa, K.; Helton, M. E.; Karlin, K. D.; Solomon, E. I. *J. Am. Chem. Soc.* **2003**, *125*, 6394). Comparison of these data to those for other relevant species revealed a remarkable degree of S–S bond activation in the compounds supported by the β-diketiminate and anilido-imine ligands, which through strong electron donation increase backbonding from the copper ions into the S–S σ* orbital and cause S–S bond weakening. Reactions of one of the complexes supported by an anilido-imine ligand with PPh_3 and xylyl isocyanide were explored, revealing facile transfer of sulfur to PPh_3 but only displacement of sulfur to yield a LCu(I)–CNAr (Ar = xylyl) complex with the isocyanide.

Introduction

Copper ions coordinated by multiple histidine N-donor and sulfur-containing thiolate or sulfide ligands comprise the active sites of numerous functionally important metalloproteins. Much interest has focused on the mononuclear type 1 and binuclear Cu_A electron-transfer sites,[1,2] for which the significance of highly covalent copper(II)−thiolate interactions has been demonstrated through detailed structural, spectroscopic, and synthetic modeling studies.[2,3] Copper(I)−thiolate centers also are prevalent in proteins that store and transport copper, as well as those that regulate gene transcription to ensure proper copper ion homeostasis.[4−6] Although ubiquitous in the biochemistry of iron,[7] sulfide has only been identified in one copper-containing enzyme, nitrous oxide reductase (N_2OR), which produces N_2 during microbial denitrification.[8] Recent structural[9] and spectroscopic[8,10] studies have revealed the catalytic site of N_2OR ("Cu_Z") to contain a novel (μ_4-sulfido)tetracopper cluster ligated by multiple histidine donors. This cluster can exist in multiple oxidation states, the most important of which appear to be the fully reduced $Cu(I)_4$ and mixed-valent $Cu(I)_xCu(II)_{4-x}$ forms.[10,11] Provocative mechanistic proposals for the enzyme

* To whom correspondence should be addressed. E-mail: tolman@chem.umn.edu.

(1) Lu, Y. In *Comprehensive Coordination Chemistry II*; McCleverty, J. A., Meyer, T. J., Eds.; Elsevier: Amsterdam, 2004; Vol. 8, pp 91−122.
(2) For selected lead references, see: (a) Randall, D. W.; Gamelin, D. R.; LaCroix, L. B.; Solomon, E. I. *J. Biol. Inorg. Chem.* **2000**, *5*, 16−19. (b) Gray, H. B.; Malmstrom, B. G.; Williams, R. J. P. *J. Biol. Inorg. Chem.* **2000**, *5*, 551−559. (c) Solomon, E. I.; Szilagyi, R. K.; DeBeer-George, S.; Basumallick, L. *Chem. Rev.* **2004**, *104*, 419−458.
(3) Tolman, W. *J. Biol. Inorg. Chem.* **2006**, *11*, 261−271 and references therein.
(4) (a) Henkel, G.; Krebs, B. *Chem. Rev.* **2004**, *104*, 801−824. (b) González-Duarte, P. In *Comprehensive Coordination Chemistry II*; McCleverty, J. A., Meyer, T. J., Eds.; Elsevier: Amsterdam, 2004; Vol. 8, pp 213−228.
(5) Rosenzweig, A. C. *Acc. Chem. Res.* **2001**, *34*, 119−128.
(6) Gaggelli, E.; Kozlowski, H.; Valensin, D.; Valensin, G. *Chem. Rev.* **2006**, *106*, 1995−2044.
(7) (a) Beinert, H.; Holm, R. H.; Münck, E. *Science* **1997**, *277*, 653−659. (b) Beinert, H. *J. Biol. Inorg. Chem.* **2000**, *5*, 2−15. (c) Holm, R. H. In *Comprehensive Coordination Chemistry II*; McCleverty, J. A., Meyer, T. J., Eds.; Elsevier: Amsterdam, 2004; Vol. 8, pp 61−90.
(8) Chen, P.; Gorelsky, S. I.; Ghosh, S.; Solomon, E. I. *Angew. Chem., Int. Ed.* **2004**, *43*, 4132−4140.
(9) (a) Brown, K.; Djinovic-Carugo, K.; Haltia, T.; Cabrito, I.; Saraste, M.; Moura, J. J. G.; Moura, I.; Tegoni, M.; Cambillau, C. *J. Biol. Chem.* **2000**, *275*, 41133−41136. (b) Haltia, T.; Brown, K.; Tegoni, M.; Cambillau, C.; Saraste, M.; Mattila, K.; Djinovic-Carugo, K. *Biochem. J.* **2003**, *369*, 77−88.

10.1021/ic061589r CCC: $37.00
Published on Web 12/14/2006

have been put forth using computational methods,[8,12] key features of which include unusual side-on coordination of N_2O to an edge of the $Cu(I)_4$ form of the cluster and μ_4-sulfide-mediated electron delocalization in higher oxidation states. Stimulated by the unusual properties of and the mechanistic hypotheses put forth for the (μ_4-sulfido)tetracopper site of N_2OR, we have begun to explore the sulfur chemistry of copper complexes supported by N-donor ligands.[13] We aim to provide fundamental chemical insights into the properties of copper−sulfur species in general and, in particular, into less common ones[14] that feature copper in oxidation states greater than +1. An ultimate goal is to prepare useful models of the N_2OR catalytic site with which to evaluate its spectroscopic properties and reactivity.[15]

Previous synthetic efforts have yielded sulfur-containing Cu(II or III) products with either the S−S bond intact (e.g., disulfido(2−), **1** and **2**,[16−18] or disulfido(·1−), **3**[13c]) or broken (e.g., sulfide, **4**),[13b] depending on the nature of the N-donor ligand and the reaction conditions (Figure 1). The μ-η^1:η^1- and μ-η^2:η^2-disulfidodicopper complexes **1**[16] and **2** (L = Tp^{iPr2} or Me_2NPY2)[17,18] are close counterparts of peroxodicopper analogs with identical tetra- or tridentate supporting ligands,[19−21] and the bonding interactions in the Cu_2O_2 and Cu_2S_2 cores are similar as determined from comparative spectroscopic/theoretical studies.[22] The side-on μ-η^2:η^2 com-

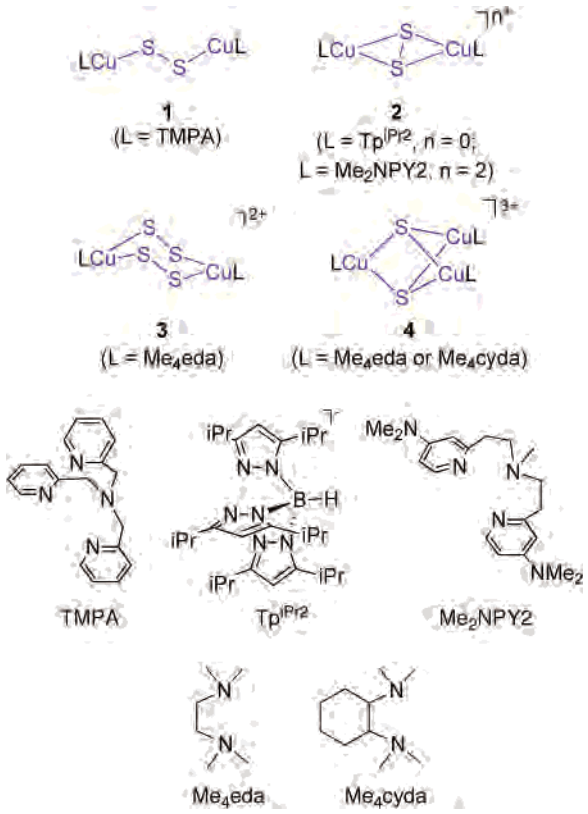

Figure 1. Copper(II or III)−sulfur complexes.

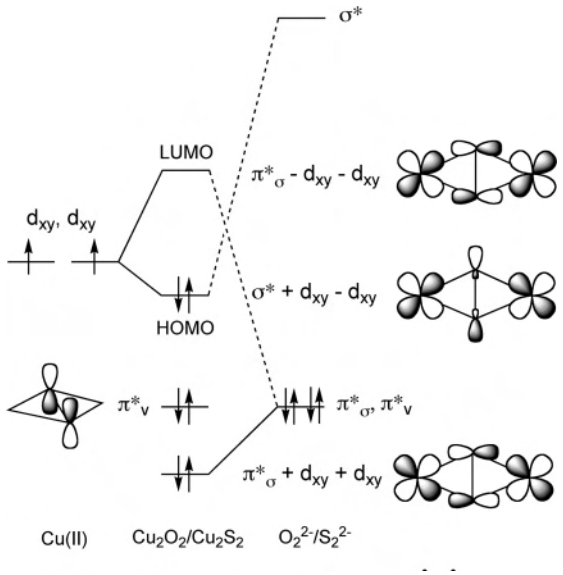

Figure 2. Schematic molecular orbital energy-level diagram for the (μ-η^2:η^2-peroxo/sulfido)dicopper core (adapted from ref 22).

plexes most pertinent here (**2**, L = Tp^{iPr2}, and its peroxo congener) exhibit a pair of intense charge-transfer (CT) electronic absorption bands and low S−S and O−O stretching frequencies of 500 and ∼760 cm^{-1}, respectively, that indicate weak bonds (i.e., extensive activation of the S_2 and O_2 moieties). These features have been rationalized by a common core-bonding model illustrated in Figure 2.[22] According to this picture, the O_2^{2-}/S_2^{2-} π^* orbital that lies in the plane of the Cu_2O_2/Cu_2S_2 core (π^*_σ) interacts strongly with the Cu d_{xy} orbitals, while the out-of-plane O_2^{2-}/S_2^{2-}

(10) (a) Rasmussen, T.; Berks, B. C.; Sanders-Loeh, J.; Dooley, D. M.; Zumft, W. G.; Thomson, A. J. *Biochemistry* **2000**, *39*, 12753−12756. (b) Alvarez, M. L.; Ai, J.; Zumft, W.; Sanders-Loeh, J.; Dooley, D. M. *J. Am. Chem. Soc.* **2001**, *123*, 576−587. (c) Chen, P.; DeBeer, G. S.; Cabrito, I.; Antholine, W. E.; Moura, J. J. G.; Moura, I.; Hedman, B.; Hodgson, K. O.; Solomon, E. I. *J. Am. Chem. Soc.* **2002**, *124*, 744−745. (d) Chen, P.; Cabrito, I.; Moura, J. J. G.; Moura, I.; Solomon, E. I. *J. Am. Chem. Soc.* **2002**, *124*, 10497−10507. (e) Oganesyan, V. S.; Rasmussen, T.; Fairhurst, S.; Thomson, A. J. *Dalton Trans.* **2004**, 996−1002.
(11) (a) Ghosh, S.; Gorelsky, S. I.; Chen, P.; Cabrito, I.; Moura, J. J. G.; Moura, I.; Solomon, E. I. *J. Am. Chem. Soc.* **2003**, *125*, 15708−15709. (b) Chan, J. M.; Bollinger, J. A.; Grewell, C. L.; Dooley, D. M. *J. Am. Chem. Soc.* **2004**, *126*, 3030−3031.
(12) Gorelsky, S. I.; Ghosh, S.; Solomon, E. I. *J. Am. Chem. Soc.* **2006**, *128*, 278−290.
(13) (a) Brown, E. C.; Aboelella, N. W.; Reynolds, A. M.; Aullón, G.; Alvarez, S.; Tolman, W. B. *Inorg. Chem.* **2004**, *43*, 3335−3337. (b) Brown, E. C.; York, J. T.; Antholine, W. E.; Ruiz, E.; Alvarez, S.; Tolman, W. B. *J. Am. Chem. Soc.* **2005**, *127*, 13752−13753. (c) York, J. T.; Brown, E. C.; Tolman, W. B. *Angew. Chem., Int. Ed.* **2005**, *44*, 7745−7748.
(14) Cu(I)−sulfur complexes are numerous, see ref 4a and (a) Dance, I. G. *Polyhedron* **1986**, *5*, 1037−1104. (b) Ramli, E.; Rauchfuss, T. B.; Stern, C. L. *J. Am. Chem. Soc.* **1990**, *112*, 4043−4044. (c) Yam, V. W.-W.; Lo, K. K.-W.; Wang, C.-R.; Cheung, K.-K., *J. Phys. Chem. A* **1997**, *101*, 4666−4672. (d) Lee, Y.; Sarjeant, A. A. N.; Karlin, K. D. *Chem. Commun.* **2006**, 621−623.
(15) Karlin, K. D. *Science* **1993**, *261*, 701−708.
(16) Helton, M. E.; Chen, P.; Paul, P. P.; Tyeklar, Z.; Sommer, R. D.; Zakharov, L. N.; Rheingold, A. L.; Solomon, E. I.; Karlin, K. D. *J. Am. Chem. Soc.* **2003**, *125*, 1160−1161.
(17) Fujisawa, K.; Moro-oka, Y.; Kitajima, N. *J. Chem. Soc., Chem. Commun.* **1994**, 623−624.
(18) Helton, M. E.; Maiti, D.; Zakharov, L. N.; Rheingold, A. L.; Porco, J. A., Jr.; Karlin, K. D. *Angew. Chem., Int. Ed.* **2006**, *45*, 1138−1141.
(19) Tyeklar, Z.; Jacobson, R. R.; Wei, N.; Murthy, N. N.; Zubieta, J.; Karlin, K. D. *J. Am. Chem. Soc.* **1993**, *115*, 2677−2689.
(20) Kitajima, N.; Fujisawa, K.; Fujimoto, C.; Moro-oka, Y.; Hashimoto, S.; Kitagawa, T.; Toriumi, K.; Tatsumi, K.; Nakamura, A. *J. Am. Chem. Soc.* **1992**, *114*, 1277−1291.
(21) Henson, M. J.; Vance, M. A.; Zhang, C. X.; Liang, H.-C.; Karlin, K. D.; Solomon, E. I. *J. Am. Chem. Soc.* **2003**, *125*, 5186−5192.
(22) Chen, P.; Fujisawa, K.; Helton, M. E.; Karlin, K. D.; Solomon, E. I. *J. Am. Chem. Soc.* **2003**, *125*, 6394−6408.

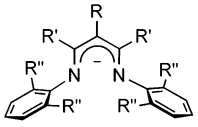

$R(R'_2L^{R''2})^-$

ligand	R	R'	R''
a	H	Me	Me
b	H	Me	Et
c	H	tBu	iPr
d	Ph	H	Et
e	Ph	H	iPr
f	3,5-$(CF_3)_2C_6H_3$	H	Me
g	3,5-$(CF_3)_2C_6H_3$	H	iPr

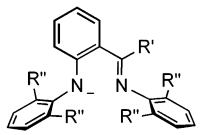

$(R'L^{'R''2})^-$

ligand	R'	R''
h	H	Me
i	H	iPr
j	Me	iPr

Figure 3. Ligands and abbreviations used in this work.

π^* orbital (π^*_v) remains basically unperturbed (nonbonding with respect to the Cu ions). The Cu−O/S bonding is thus dominated by highly covalent, strong σ-donation from the filled O_2^{2-}/S_2^{2-} π^*_σ orbital into the Cu d_{xy} set. An additional interaction occurs between the Cu d_{xy} orbitals and the empty O_2^{2-}/S_2^{2-} σ^* orbital. Essentially a backbonding interaction, it results in a lowering of the predominantly Cu-based HOMO energy and rationalizes the weakening of the O_2^{2-}/S_2^{2-} bond. The electronic CT absorption bands derive from excitations out of the $\pi^*_\sigma + xy + xy$ and π^*_v orbitals, with the former being more intense and at higher energy. A detailed comparative study[22] showed that the Cu_2S_2 core of **2** (L = Tp^{iPr2}) exhibits greater metal−ligand covalency (π^*_σ/Cu) and backbonding (Cu/σ^*) than its peroxide analog, corresponding to a more significant weakening (activation) of the S−S bond.[22]

We recently communicated the synthesis and characterization of two examples of μ-η^2:η^2-disulfide complexes supported by bidentate N-donor ligands (**2**, L = **b** or **i**, Figure 3).[13a] Their S−S bond distances (2.2007(11) and 2.165(3) Å, respectively) are distinctly longer than that of **2**, L = Tp^{iPr2} or Me_2NPY2, (2.073(4) Å and 2.117(2) Å, respectively), suggesting an even greater degree of S−S bond weakening because of the nature of the supporting ligands. Here, we present a more complete study in which we assess the X-ray structures, UV−vis and resonance Raman spectra, and aspects of the reactivity of a series of μ-η^2:η^2-disulfide complexes supported by bidentate N-donor ligands with variable steric and electronic properties (Figure 3). Interpretations of the spectroscopic properties within the context of the bonding picture illustrated in Figure 2, correlations of Cu_2S_2 core structural parameters and S−S stretching frequencies, and reactivity different from that previously reported for **2**, L = Me_2NPY2 (Figure 1)[18] are discussed. Taken together, these results provide new insights into ligand influences on S−S bond activation by copper ions.

Experimental Section

General Considerations. All solvents and reagents were obtained from commercial sources and used as received unless noted otherwise. The solvents tetrahydrofuran (THF), pentane, diethyl ether (Et_2O), acetonitrile (CH_3CN), and CH_2Cl_2 were passed though solvent purification columns (Glass Contour, Laguna, CA, or MBraun) prior to use. All metal complexes were prepared and stored in a Vacuum Atmospheres inert atmosphere glove box under a dry nitrogen atmosphere or were manipulated using standard Schlenk line techniques. Labeled elemental sulfur (^{34}S, 99% enrichment) was purchased from Cambridge Isotope Laboratories, Inc. Complexes of the general formula $R(R'L^{R''2})Cu(CH_3CN)$,[23] as well as $(HL'^{iPr2})Cu(CH_3CN)$,[24] $(MeL'^{iPr2})Cu(CH_3CN)$,[25] $[H(Me_2L^{Et2})Cu]_2(S_2)$ (**2b**),[13a] and $[(HL'^{iPr2})Cu]_2(S_2)$ (**2i**),[13a] were prepared via previously reported methods (for ligand nomenclature, see Figure 3). The complex $(HL'^{Me2})Cu$ was prepared similarly to $(HL'^{iPr2})Cu(CH_3CN)$, characterized by ^1H NMR spectroscopy, and used directly for the synthesis of $[(HL'^{Me2})Cu]_2(S_2)$ (**2h**) (Supporting Information).

Physical Methods. NMR spectra were recorded on a Varian VI-300 or VXR-300 spectrometer. Chemical shifts (δ) for ^1H NMR spectra were referenced to residual protium in the deuterated solvent. UV−vis spectra were recorded on a HP8453 (190−1100 nm) diode array spectrophotometer; extinction coefficients were determined from Beers' Law plots. Resonance Raman spectra were recorded on an Acton 506 spectrometer using a Princeton Instruments LN/CCD-11100-PB/UVAR detector and ST-1385 controller interfaced with Winspec software. A Spectra Physics BeamLok 2065-7S Ar Laser provided excitation at 457.9 nm. The spectra were obtained at −196 °C using a backscattering geometry. Samples were frozen in NMR tubes in thermal contact with a Dewar flask containing liquid nitrogen. Raman shifts were externally referenced to liquid indene. Elemental analyses were performed by Robertson Microlit (Madison, NJ).

$[H(Me_2L^{Me2})Cu]_2(S_2)$ (2a). $[H(Me_2L^{Me2})]Cu(CH_3CN)$ (43.6 mg, 0.12 mmol) in CH_3CN (4 mL) was added to elemental sulfur (3.8 mg, 0.015 mmol) in CH_3CN (2 mL). The reaction mixture was stirred for 30 min, during which a brown precipitate formed. The precipitate was collected, washed with CH_3CN (4 mL), and dried under reduced pressure (13.4 mg, 44%). Allowing the reaction mixture to stir for >1 h resulting in the conversion of $[H(Me_2L^{Me2})Cu]_2(S_2)$ to $[Cu(SR)]_4$ [R = $H(Me_2L^{Me2})$] (**5a**); a ^1H NMR spectrum of this residue matched that of **5a** prepared independently (see below). ^1H NMR (C_6D_6, 300 MHz): δ 6.90−7.01 (m, 12H), 4.79 (s, 2H), 2.03 (s, 24H), 1.44 (s, 12 H). UV−vis (THF) [λ_{max}, nm (ϵ, M^{-1} cm^{-1})]: 211 (18500), 327 (19200), 352 (12000), 427 (8200), 540 (400), 804 (130). Repeated attempts to obtain a satisfactory elemental analysis (CHN) for **2a** failed; we attribute this to the variable small amounts of sulfur impurities that we were unable to remove by recrystallization because of the competing formation of **5a**. Structural assignment thus rests on the X-ray crystal structure and the spectroscopic data.

$[H(tBu_2L^{iPr2})Cu]_2(S_2)$ (2c). $[H(tBu_2L^{iPr2})]Cu(CH_3CN)$ (45.3 mg, 0.075 mmol) in pentane (3 mL) was added to elemental sulfur (1.2

(23) Spencer, D. J. E.; Reynolds, A. M.; Holland, P. J.; Jazdzewski, B. A.; Duboc-Toia, C.; Le Pape, L.; Yokota, S.; Tachi, Y.; Itoh, S.; Tolman, W. B. *Inorg. Chem.* **2002**, *41*, 6307−6321.
(24) Hayes, P. G.; Welch, G. C.; Emslie, D. J. H.; Noack, C. L.; Piers, W. E.; Parvez, M. *Organometallics* **2003**, *22*, 1577−1579.
(25) Reynolds, A. M.; Gherman, B. F.; Cramer, C. J.; Tolman, W. B. *Inorg. Chem.* **2005**, *44*, 6989−6997.

mg, 0.0047 mmol) in pentane (2 mL). The reaction mixture was stirred for 1 h and filtered though Celite, and the filtrate was concentrated under reduced pressure to ~2 mL. Storage of the orange solution at −20 °C resulted in the formation of yellow and brown crystals in a ratio of about 30:1. The brown material was identified as $[H(tBu_2L^{iPr2})Cu]_2(S_2)$ by X-ray crystallography on a selected crystal, but a pure bulk sample has not been obtained to date. Raman spectroscopy was performed on an initial reaction solution prepared in benzene, which was frozen in liquid N_2 immediately after preparation.

$[Ph(H_2L^{Et2})Cu]_2(S_2)$ (2d). $[Ph(H_2L^{Et2})]Cu(CH_3CN)$ (112.0 mg, 0.22 mmol) in CH_3CN (5 mL) was added to elemental sulfur (7.0 mg, 0.027 mmol) in CH_3CN (2 mL). The reaction mixture was stirred for 3 h, during which a green precipitate formed. The precipitate was collected, washed with CH_3CN (8 mL), and dried under reduced pressure (88.7 mg, 40%). ^1H NMR (C_6D_6, 300 MHz): δ 7.58 (s, 4H), 6.92−7.11 (m, 22 H), 2.51 (quartet, J = 7.5 Hz, 16H), 1.07 (t, J = 7.5 Hz, 24H). UV−vis (THF) [λ_{max}, nm (ϵ, $M^{-1}cm^{-1}$)]: 295 (49385), 387 (34376), 421 (23470), 588 (1260), 813 (310). Anal. Calcd for $C_{58}H_{66}Cu_2N_4S_2$: C, 68.95; H, 6.58; N, 5.55. Found: C, 68.67; H, 6.43; N, 5.40.

$[Ph(H_2L^{iPr2})Cu]_2(S_2)$ (2e). $[Ph(H_2L^{iPr2})]Cu(CH_3CN)$ (46.5 mg, 0.082 mmol) in CH_3CN (3 mL) was added to elemental sulfur (2.6 mg, 0.01 mmol) in CH_3CN (2 mL). The reaction mixture was stirred for 2 h, during which a green precipitate formed. The precipitate was collected, washed with CH_3CN (8 mL), and dried under reduced pressure (32.0 mg, 70%). ^1H NMR (C_6D_6, 300 MHz): δ 7.66 (s, 4 H), 7.04−7.22 (m, 14 H), 6.98 (d, J = 7.6 Hz, 8 H), 3.26 (septet, J = 6.9 Hz, 8 H), 1.06 (d, J = 6.8 Hz, 24 H), 1.01 (d, J = 6.8 Hz, 24 H). UV−vis (THF) [λ_{max}, nm (ϵ, M^{-1} cm^{-1})]: 299 (52 760), 386 (32 410), 432 (24 350), 612 (1290). Anal. Calcd for $C_{66}H_{82}Cu_2N_4S_2$: C, 70.61; H, 7.36; N, 4.99. Found: C, 70.32; H, 7.62; N, 4.72.

$[3,5\text{-}(CF_3)_2C_6H_3(H_2L^{Me2})Cu]_2(S_2)$ (2f). $[3,5\text{-}(CF_3)_2C_6H_3(H_2L^{Me2})]Cu(CH_3CN)$ (65.2 mg, 0.11 mmol) in CH_3CN (4 mL) was added to elemental sulfur (3.5 mg, 0.014 mmol) in CH_3CN (3 mL). The reaction mixture was stirred for 4 h, during which a brown precipitate formed. The precipitate was collected, washed with CH_3CN (5 mL), and dried under reduced pressure (38.0 mg, 59%). ^1H NMR (C_6D_6, 300 MHz): δ 7.56 (s, 2H), 7.41 (s, 4H), 7.26 (s, 4H), 6.96 (m, 4H), 6.88 (d, J = 7.4 Hz, 8H), 1.99 (s, 24H). UV−vis (THF) [λ_{max}, nm (ϵ, M^{-1} cm^{-1})]: 319 (60 500), 377 (32 900), 421 (25 500), 547 (1400), 827 (600). Anal. Calcd for $C_{54}H_{46}Cu_2F_{12}N_4S_2$: C, 55.43; H, 3.96; N, 4.79. Found: C, 55.16; H, 4.23; N, 4.58.

$[3,5\text{-}(CF_3)_2C_6H_3(H_2L^{iPr2})Cu]_2(S_2)$ (2g). $[3,5\text{-}(CF_3)_2C_6H_3(H_2L^{iPr2})]Cu(CH_3CN)$ (190.0 mg, 0.27 mmol) in CH_3CN (6 mL) was added to elemental sulfur (8.6 mg, 0.034 mmol) in CH_3CN (3 mL). The reaction mixture was stirred for 2 h, during which a green precipitate formed. The precipitate was collected, washed with CH_3CN (2 × 6 mL), and dried under reduced pressure (172.0 mg, 91%). ^1H NMR (C_6D_6, 300 MHz): δ 7.67 (s, 4H), 7.60 (s, 4H), 7.53 (s, 2H), 7.11 (t, J = 7.9 Hz, 4H), 6.94 (d, J = 7.86 Hz, 8H), 3.19 (septet, J = 6.58 Hz, 8H), 1.02 (apparent t: two overlapping d, J = 6.58 Hz, 48H). UV−vis (THF) [λ_{max}, nm (ϵ, M^{-1} cm^{-1})]: 322 (54 300), 381 (26 200), 434 (22 800), 575 (1300), 830 (290). Anal. Calcd for $C_{70}H_{78}Cu_2F_{12}N_4S_2$: C, 60.29; H, 5.64; N, 4.02. Found: C, 59.99; H, 5.52; N, 3.95.

$[(HL'^{Me2})Cu]_2(S_2)$ (2h). $(HL'^{Me2})Cu(CH_3CN)$ (102.0 mg, 0.24 mmol) in CH_3CN (4 mL) was added to elemental sulfur (7.6 mg, 0.03 mmol) in CH_3CN (2 mL). The reaction mixture was stirred for 3 h, during which a green precipitate formed. The precipitate was collected, washed with CH_3CN (6 mL), and dried under reduced pressure (67.0 mg, 67%). ^1H NMR (C_6D_6, 300 MHz): δ 7.41 (s, 2H), 6.96−7.07 (m, 8H), 6.77−6.89 (m, 8H), 6.36 (d, J = 8.4 Hz, 2H), 6.26 (m, 2H), 2.09 (s, 12H), 1.91 (s, 12 H). UV−vis (THF) [λ_{max}, nm (ϵ, M^{-1} cm^{-1})]: 256 (49 700), 282 (31 300), 435 (29 100), 604 (1300), 815 (400). Anal. Calcd for $C_{46}H_{46}Cu_2N_4S_2$: C, 65.30; H, 5.48; N, 6.62. Found: C, 64.83; H, 5.42; N, 6.49.

$[(MeL'^{iPr2})Cu]_2(S_2)$ (2j). $(MeL'^{iPr2})Cu(CH_3CN)$ (51.8 mg, 0.09 mmol) in toluene (5 mL) was added to elemental sulfur (3.0 mg, 0.012 mmol) in toluene (2 mL). The reaction mixture was stirred for 3 h and filtered though Celite, and the volume was reduced to 2 mL. The addition of 20 mL of CH_3CN and storage at −20 °C resulted in the precipitation of a dark green solid. The green solid was collected and dried under reduced pressure (17.0 mg, 33%). ^1H NMR (C_6D_6, 300 MHz): δ 7.40 (d, J = 9.6 Hz, 2H), 6.85−7.30 (m, 12 H), 6.80 (m, 2H), 6.41 (d, J = 8.7 Hz, 2H), 6.31 (m, 2H), 3.25 (septet, J = 6.6 Hz, 4H), 2.87 (septet, J = 6.6 Hz, 4H), 1.85 (s, 6H), 1.22 (m, 24H), 1.12 (d, J = 6.9 Hz, 12H), 0.97 (d, J = 6.9 Hz, 12H). UV−vis (THF) [λ_{max}, nm (ϵ, M^{-1} cm^{-1})]: 250 (32 200), 292 (15 800), 437 (17 700), 460 (21 600), 651 (1000), 877 (120). Anal. Calcd for $C_{64}H_{82}Cu_2N_4S_2$: C, 69.97; H, 7.52; N, 5.10. Found: C, 69.35; H, 7.06; N, 4.62.

$[Cu(SR)]_4$ [R = $H(Me_2L^{Me2})$] (5a). $H(Me_2L^{Me2})Cu(CH_3CN)$ (90.0 mg, 0.22 mmol) in a 1:1 toluene/CH_3CN (4 mL) solution was added to elemental sulfur (7.14 mg, 0.028 mmol) in CH_3CN (2 mL). The reaction mixture was stirred for 2 h, resulting in the development of a tan precipitate. The solid was collected, washed with CH_3CN (3 × 5 mL), and dried under reduced pressure (50 mg, 57%). ^1H NMR (CD_2Cl_2, 300 MHz): δ 6.80−7.00 (m, 24H), 3.90 (s, 4H), 2.09 (broad s, 24H), 2.03 (broad s, 12H), 1.96 (broad s, 12 H), 1.73 (broad s, 12 H), 1.65 (broad s, 12H). Anal. Calcd for $C_{84}H_{100}Cu_4N_8S_4$: C, 62.89; H, 6.28; N, 6.99. Found: C, 62.47; H, 5.85; N, 6.88.

Reactions of 2h with PPh_3. Two equivalents of PPh_3 (7.1 mg, 0.027 mmol) were dissolved in C_6D_6 (1 mL), and the mixture was added to $[(HL'^{Me2})Cu]_2(S_2)$ (**2h**) (11.4 mg, 0.013 mmol). After the mixture was stirred for 1 h, ^1H and $^{31}P\{^1H\}$ NMR spectra were obtained, which showed formation of 1 equiv of triphenylphosphine sulfide, 1 equiv of $(HL'^{Me2})Cu(PPh_3)$, and 0.5 equiv of unreacted **2h**. The identity of $(HL'^{Me2})Cu(PPh_3)$ was confirmed by independently reacting $(HL'^{Me2})Cu(CH_3CN)$ (9.2 mg, 0.021 mmol) with PPh_3 (5.6 mg, 0.021 mmol) in C_6D_6 (1 mL). ^1H NMR (C_6D_6, 300 MHz): δ 7.97 (d, J = 2.7 Hz, 1H), 6.80−7.10 (m, 23H), 6.66 (d, J = 8.7 Hz, 1H), 6.41 (t, J = 7.6 Hz, 1H), 2.23 (s, 6H), 2.03 (s, 6H). $^{31}P\{^1H\}$ NMR (C_6D_6, 121.372 MHz): δ 6.81. A similar reaction of PPh_3 with **2h**, using 4 equiv of phosphine, yielded 2 equiv of triphenylphosphine sulfide and 2 equiv of $(HL'^{Me2})Cu(PPh_3)$.

Reaction of 2h with Xylyl Isocyanide. Two equivalents of xylyl isocyanide (3.7 mg, 0.028 mmol) were dissolved in C_6D_6 (1 mL) and added to $[(HL'^{Me2})Cu]_2(S_2)$ (**2h**) (12.0 mg, 0.014 mmol). After the mixture was stirred for 1 h, the only species observed by ^1H NMR spectroscopy was the Cu(I)−xylyl isocyanide adduct. The identity of this adduct was confirmed by independently reacting $(HL'^{Me2})Cu(CH_3CN)$ (11.4 mg, 0.026 mmol) with xylyl isocyanide (3.5 mg, 0.026 mmol) in C_6D_6 (1 mL). ^1H NMR (C_6D_6, 300 MHz): δ 7.96 (s, 1H), 6.90−7.30 (m, 8H), 6.68 (d, J = 8.7 Hz, 1H), 6.59 (t, J = 7.5 Hz, 1H), 6.43 (t, J = 7.0 Hz, 1H), 6.39 (d, J = 7.8 Hz, 2H), 2.48 (s, 6H), 2.31 (s, 6H), 1.65 (s, 6H).

X-ray Crystallography. Crystals of the appropriate size were chosen and placed on the tip of a 0.1 mm diameter glass fiber and mounted on a Siemens SMART Platform CCD diffractometer for data collection at 173(2) K. Data collections were carried out using Mo Kα radiation (graphite monochomator) with a detector distance

Scheme 1. Synthesis of Complexes

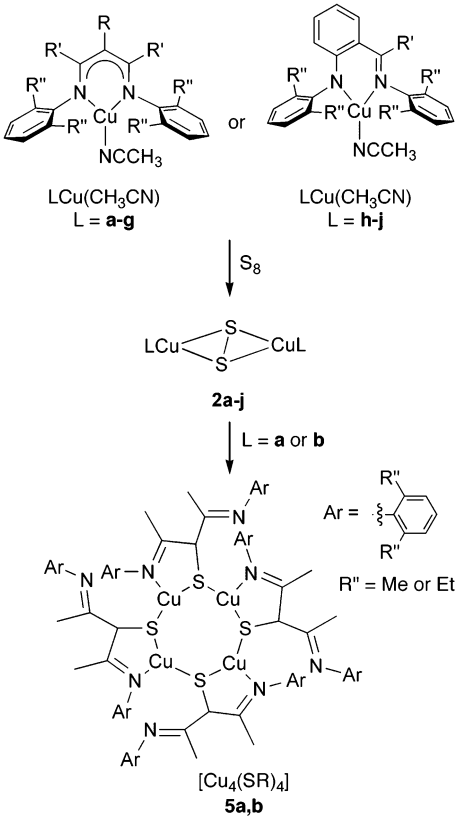

of 4.9 cm. The intensity data were corrected for absorption and decay (SADABS).[26] Final cell constants were calculated from the *xyz* centroids of strong reflections from the actual data collection after integration (SAINT).[27] The CIFs given in the Supporting Information show additional crystal and refinement information. The structures were solved by direct methods using SHELXL-97[28] software. All non-hydrogen atoms were refined with anisotropic displacement parameters. All hydrogen atoms were placed in ideal positions and refined as riding atoms with relative isotropic displacement parameters. Pertinent details for each structure are noted below (see Table S1 for a summary of crystallographic data and the CIFs for full crystallographic information).

[H(Me$_2$L^{Me2})Cu]$_2$(S$_2$) (2a). Red crystals suitable for X-ray crystallography were grown by vapor diffusion of pentane into a toluene solution at −20 °C. The final full-matrix least-squares refinement converged to R1 = 0.0321 and wR2 = 0.0870 (F^2, all data).

[H(tBu$_2$L^{iPr2})Cu]$_2$(S$_2$) (2c). Red crystals suitable for X-ray crystallography were grown from pentane at −20 °C. The carbon atoms of one isopropyl group were found to be disordered over two positions with a 79:21 occupancy ratio. A pentane solvent molecule was also disordered over two positions, as well as over a 2-fold symmetry axis. Attempts to model the disorder were unsuccessful so the reflection contributions of the solvent were removed using the program PLATON, function SQUEEZE,[29] which calculated that there are 171 electrons in a volume of 852 Å^3 per unit cell. The final full-matrix least-squares refinement converged to R1 = 0.0450 and wR2 = 0.1031 (F^2, all data).

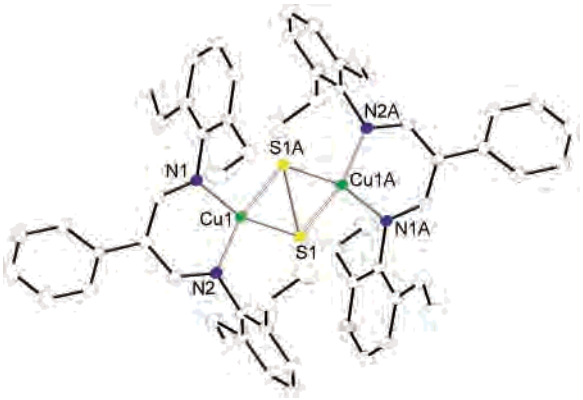

Figure 4. X-ray structure of **2d**, showing all non-hydrogen atoms as 50% thermal ellipsoids.

[Ph(H$_2$L^{Et2})Cu]$_2$(S$_2$) (2d). Green crystals suitable for X-ray crystallography were grown from pentane at −20 °C. The final full-matrix least-squares refinement converged to R1 = 0.0386 and wR2 = 0.0825 (F^2, all data).

[Ph(H$_2$L^{iPr2})Cu]$_2$(S$_2$) (2e). Green crystals suitable for X-ray crystallography were grown by vapor diffusion of pentane into a toluene solution at −20 °C. The carbon atoms of one isopropyl group were found to be disordered over two positions with a 52:48 occupancy ratio. Two molecules of toluene are also present within the asymmetric unit. The final full-matrix least-squares refinement converged to R1 = 0.0348 and wR2 = 0.0747 (F^2, all data).

[3,5-(CF$_3$)$_2$C$_6$H$_3$(H$_2$L^{Me2})Cu]$_2$(S$_2$) (2f). Brown crystals suitable for X-ray crystallography were grown from vapor diffusion of pentane into a CH_2Cl_2 solution at −20 °C. The fluorine atoms of one of the CF_3 groups were found to be disordered over two positions with an 84:16 occupancy ratio. The final full-matrix least-squares refinement converged to R1 = 0.0419 and wR2 = 0.0962 (F^2, all data).

[3,5-(CF$_3$)$_2$C$_6$H$_3$(H$_2$L^{iPr2})Cu]$_2$(S$_2$) (2g). Green crystals suitable for X-ray crystallography were grown from pentane at −20 °C. The fluorine atoms of one of the CF_3 groups were found to be disordered over two positions with a 90:10 occupancy ratio. Highly disordered solvent was found that could not be modeled appropriately. The reflection contributions of the solvent were removed using the program PLATON, function SQUEEZE,[29] from which it was determined that there were 143 electrons in a volume of 578.3 Å^3 per unit cell. The final full-matrix least-squares refinement converged to R1 = 0.0380 and wR2 = 0.1039 (F^2, all data).

[(HL'^{Me2})Cu]$_2$(S$_2$) (2h). Green crystals suitable for X-ray crystallography were grown by vapor diffusion of pentane into a toluene solution at −20 °C. Two molecules of toluene are present within the asymmetric unit. The final full-matrix least-squares refinement converged to R1 = 0.0410 and wR2 = 0.0997 (F^2, all data).

[(MeL'^{iPr2})Cu]$_2$(S$_2$) (2i). Green crystals suitable for X-ray crystallography were grown from pentane at −20 °C. Highly disordered solvent was found that could not be modeled appropriately. The reflection contributions of the solvent were removed using the program PLATON, function SQUEEZE,[29] from which it was determined that there were 283 electrons in a volume of 1484 Å^3 per unit cell. The final full-matrix least-squares refinement converged to R1 = 0.0446 and wR2 = 0.1183 (F^2, all data).

(26) For an empirical correction for absorption anisotropy, see: Blessing, R. *Acta Crystallogr.* **1995**, *A51*, 33.
(27) *SAINT*, version 6.2; Bruker Analytical X-Ray Systems: Madison, WI, 2001.
(28) *SHELXTL*, version 6.10; Bruker Analytical X-Ray Systems: Madison, WI, 2000.
(29) Spek, A. L. *Platon, A Multipurpose Crystallographic Tool*; Utrecht University: Utrecht, The Netherlands, 2002.

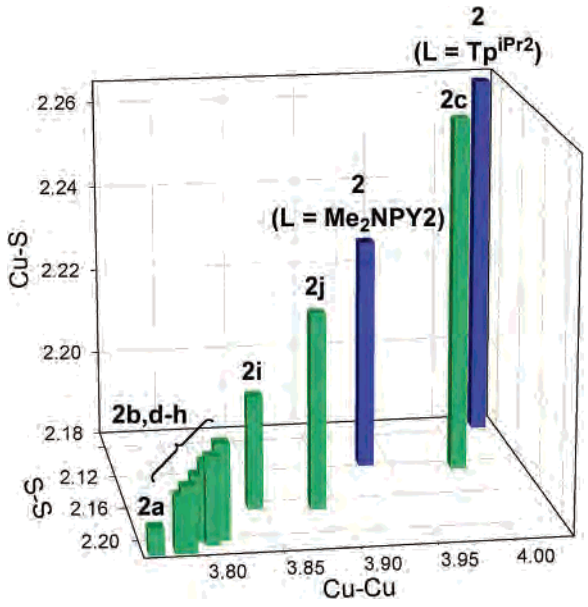

Figure 5. Plot of Cu−Cu, S−S, and Cu−S distances (Å, from Table 2) determined by X-ray crystallography for the μ-η^2:η^2-disulfidodicopper complexes (blue = complexes supported by tri- and tetradentate ligands; green = complexes supported by bidentate β-diketiminate and anilido-imine ligands). For label nomenclature, see Figures 1 and 3.

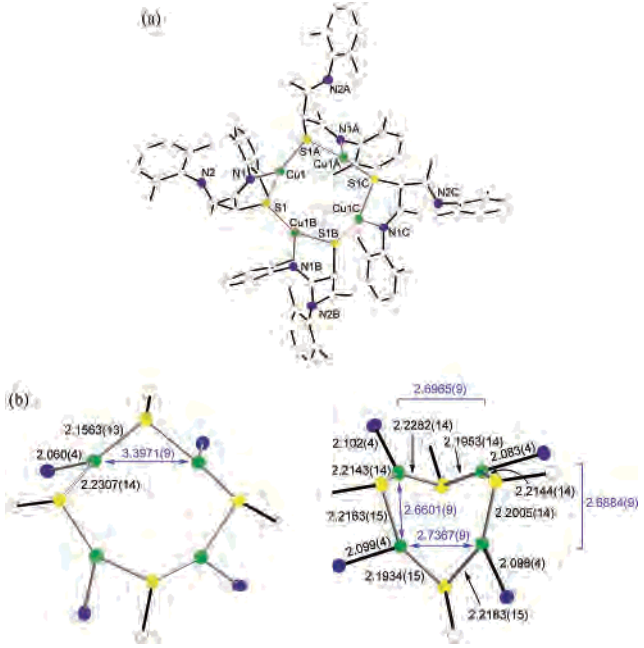

Figure 6. (a) X-ray structure of [Cu(SR)]$_4$ (R = H(Me$_2$L^{Me2})), showing all non-hydrogen atoms as 50% thermal ellipsoids. (b) Comparison of the cores of the structures of [Cu(SR)]$_4$ (left, R = H(Me$_2$L^{Me2}); right, H(Me$_2$L^{Et2})) with selected interatomic distances shown (Å): green, Cu; blue, N; yellow, S; white, C. Note that the complex on the left features a C_4 axis, so only one set of unique distances are listed.

[Cu(SR)]$_4$ [R = H(Me$_2$L^{Me2})] (5a). Yellow crystals suitable for X-ray crystallography were grown by vapor diffusion of pentane into a CH_2Cl_2 solution at −20 °C. Highly disordered solvent was found that could not be modeled appropriately. The reflection contributions of the solvent were removed using the program PLATON, function SQUEEZE,[29] from which it was determined that there were 110 electrons in a volume of 1819 Å^3 per unit cell. The final full-matrix least-squares refinement converged to R1 = 0.0570 and wR2 = 0.1326 (F^2, all data).

Table 1. Selected Interatomic Distances (Å) and Angles (deg)[a]

	[H(Me$_2$L^{Me2})Cu]$_2$(S$_2$) (**2a**)		
Cu1−N1	1.8964(17)	Cu1−S1A	2.1868(6)
Cu1−N2	1.8994(17)	S1−S1A	2.2140(10)
Cu1−S1	2.1842(6)	Cu1···Cu1A	3.7687(5)
S1−Cu1−S1A	60.87(2)	N1−Cu1−S1−S1A	3.84(17)
	[H(Me$_2$L^{Et2})Cu]$_2$(S$_2$)[b] (**2b**)		
Cu1−N1	1.9065(18)	Cu1−S1A	2.1974(6)
Cu1−N2	1.9101(18)	S1−S1A	2.2007(11)
Cu1−S1	2.1930(6)	Cu1···Cu1A	3.7991(5)
S1−Cu1−S1A	60.16(3)	N−Cu1−S1−S1A	−0.07(18)
	[H(tBu$_2$L^{iPr2})Cu]$_2$(S$_2$) (**2c**)		
Cu1−N1	1.942(2)	Cu1−S2	2.2674(6)
Cu1−N2	1.936(2)	S1−S2	2.1242(13)
Cu1−S1	2.2572(6)	Cu1···Cu1A	3.9950(7)
S1−Cu1−S2	56.00(3)	N−Cu1−S1−S2	−32.40(18)
	[Ph(H$_2$L^{Et2})Cu]$_2$(S$_2$) (**2d**)		
Cu1−N1	1.910(2)	Cu1−S1A	2.1940(10)
Cu1−N2	1.909(2)	S1−S1A	2.2138(13)
Cu1−S1	2.1951(10)	Cu1···Cu1A	3.7899(12)
S1−Cu1−S1A	60.58(3)	N2−Cu1-S1−S1A	−5.0(2)
	[Ph(H$_2$L^{iPr2})Cu]$_2$(S$_2$) (**2e**)		
Cu1−N1	1.9054(16)	Cu1−S1A	2.2051(6)
Cu1−N2	1.9127(16)	S1−S1A	2.2007(10)
Cu1−S1	2.1984(6)	Cu1···Cu1A	3.8143(5)
S1−Cu1−S1A	59.97(2)	N2−Cu1−S1−S1A	−6.27(17)
	[3,5-(CF$_3$)$_2$C$_6$H$_3$(H$_2$L^{Me2})Cu]$_2$(S$_2$) (**2f**)		
Cu1−N1	1.912(2)	Cu1−S1A	2.1976(8)
Cu1−N2	1.906(2)	S1−S1A	2.2013(15)
Cu1−S1	2.1978(8)	Cu1···Cu1A	3.8045(7)
S1−Cu1−S1A	60.11(4)	N1−Cu1−S1−S1A	−4.6(3)
	[3,5-(CF$_3$)$_2$C$_6$H$_3$(H$_2$L^{iPr2})Cu]$_2$(S$_2$) (**2g**)		
Cu1−N1	1.9213(18)	Cu1−S1A	2.1941(9)
Cu1−N2	1.9047(17)	S1−S1A	2.2060(12)
Cu1−S1	2.2060(9)	Cu1···Cu1A	3.8072(10)
S1−Cu1−S1A	60.18(2)	N1−Cu1−S1−S1A	−6.3(2)
	[(HL'^{Me2})Cu]$_2$(S$_2$) (**2h**)		
Cu1−N1	1.925(2)	Cu1−S1A	2.1916(8)
Cu1−N2	1.893(2)	S1−S1A	2.2130(15)
Cu1−S1	2.1936(8)	Cu1···Cu1A	3.7858(7)
S1−Cu1−S1A	60.62(3)	N1−Cu1−S1−S1A	−6.6(2)
	[(HL'^{iPr2})Cu]$_2$(S$_2$)[b] (**2i**)		
Cu1−N1	1.880(5)	Cu1−S1A	2.2113(18)
Cu1−N2	1.922(5)	S1−S1A	2.165(3)
Cu1−S1	2.2011(18)	Cu1···Cu1A	3.8446(16)
S1−Cu1−S1A	58.78(8)	N−Cu1−S1−S1A	−3.9(5)
	[(MeL'^{iPr2})Cu]$_2$(S$_2$) (**2j**)		
Cu1−N1	1.889(2)	Cu1−S2	2.2224(6)
Cu1−N2	1.929(2)	S1−S2	2.1691(13)
Cu1−S1	2.2278(6)	Cu1···Cu1A	3.8857(8)
S1−Cu1−S2	58.34(3)	N2−Cu1−S1−S2	1.5(2)

[a] Estimated standard deviations in parentheses. "A" refers to symmetry-related atoms. [b] These structures have been reported previously.[13a]

Results

Synthesis of Complexes. With one exception, the series of μ-η^2:η^2-disulfidodicopper(II) complexes **2a**−**j** were isolated as either brown or green solids from the reaction of the Cu(I) precursors (**a**−**j**)Cu(CH$_3$CN) with S$_8$ in CH$_3$CN,

Table 2. Cu_2S_2 Core Distances (Å) and Vibrational Frequencies (cm^{-1}) for (μ-η^2:η^2-disulfido)dicopper Complexes

	S−S	Cu···Cu	av Cu−S	ν(S−S)	$\Delta\nu$(^{34}S)	ref
2a	2.214(10)	3.7687(5)	2.186	442	9	this work
2b	2.2007(11)	3.7991(5)	2.195	443	10	13a
2c	2.1242(13)	3.9950(7)	2.262	454	13	this work
2d	2.2138(13)	3.7899(12)	2.195	424	10	this work
2e	2.2007(10)	3.8143(5)	2.202	435	8	this work
2f	2.2013(15)	3.8045(7)	2.198	441	9	this work
2g	2.2060(12)	3.8072(10)	2.200	428	12	this work
2h	2.2130(15)	3.7858(7)	2.193	432	8	this work
2i	2.165(3)	3.8446(16)	2.206	440	13	13a
2j	2.1691(13)	3.8857(8)	2.225	443	11	this work
2 (L = Tp^{iPr2})	2.073(4)	4.028(3)	2.264	500	12	17, 22
2 (L = Me_2NPY2)	2.117(2)	3.9336(10)	2.233			18

toluene, or pentane (Scheme 1).[30] The products were characterized by ^{1}H NMR, UV−vis, and resonance Raman spectroscopy, as well as by CHN analysis and X-ray crystallography. The exceptional case was [H(tBu_2L^{iPr2})Cu]$_2$-(S_2) (**2c**, Figure 2), which we were unable to isolate as an analytically pure bulk sample, although crystals suitable for an X-ray structural determination were obtained. Isolation of samples of the complexes lacking a substituent on the central methine position of the β-diketiminate ligand (e.g., **2a** and **b**) required shorter reaction times to prevent conversion to the Cu(I) clusters [Cu(SR)]$_4$ (**5a** and **b**, Scheme 1), which were fully characterized in two instances (R = H(Me_2L^{Et2}), **5b**,[13a] and H(Me_2L^{Me2}), **5a**). Exclusive formation of **5a** was possible using a CH_3CN/toluene mixture as solvent and allowing the solution to stir for >1 h.

X-ray Structures. (a) Disulfido Complexes. X-ray crystal structures of **2a**−**j** were determined, with **2b** and **i** having been reported previously.[13a] Because of their general similarity, only that of **2d** is shown here (Figure 4); thermal ellipsoid representations of **2a**, **c**, **e**−**h**, and **j** are provided as Supporting Information (Figures S1−S7). Selected interactomic distances and angles for all of the complexes are summarized in Table 1.

In each complex, the copper centers are coordinated to two nitrogen atoms of the supporting ligand and both sulfur atoms of the μ-η^2:η^2-disulfido bridge in a square planar geometry. Some deviation of the Cu(II) ion from a square planar shape is observed for **2c**, presumably because of the large steric constraints of the supporting ligand. This deviation is evident by the significant distortion of the N−Cu−S−S torsion angle (N2−Cu−S1−S2 = −32.4°) from the idealized value of ∼0°. Overall, the complexes in the series exhibit similar planar Cu_2S_2 core geometries. Nonetheless, structural variation is evident upon comparison of the Cu_2S_2 core parameters (Cu−Cu, S−S, and Cu−S distances) for **2a**−**j** and other examples from the literature (Table 2, Figure 4). The plot in Figure 5 shows that the core parameters for most of the β-diketiminate complexes are clustered close to one another (lower left), but across the entire set there is a correlated trend, such that the S−S distance decreases as the Cu−Cu and Cu−S distances increase. This trend implies that as the supporting N-donor ligand is varied, the core bonding and extent of S−S bond activation changes; stronger bonding of the copper centers to the S_2^{2-} moiety accompanies a decreased S−S bond order. The relationship between the Cu_2S_2 bonding and the supporting ligand attributes is analyzed below (Discussion).

(b) Clusters [Cu(SR)]$_4$ (R = H(Me_2L^{Me2}), 5a, or H(Me_2L^{Et2}), 5b). The new X-ray structure of **5a** is presented in Figure 6a, and its core is compared to that of the previously reported complex[13a] **5b** in Figure 6b. The atom connectivity in **5a** and **5b** is the same; both complexes feature 3-coordinate Cu(I) ions bridged by thiolate sulfur atoms derived from functionalization of the original β-diketiminate ligand at the central methine carbon. The complexes adopt significantly different geometries, however, and thus can be envisioned as conformational isomers (notwithstanding the different Me vs Et substituents). As indicated in Figure 6b, the [$Cu_4(SR)_4$] core of **5a** (which features a C_4 molecular axis of symmetry) is expanded relative to the folded core of **5b**, such that the former features Cu···Cu distances ∼0.7 Å longer than in the latter. The puckering of the core in **5b** is accompanied by significantly more acute Cu−S−Cu angles (∼75°) relative to those in **5a** (∼100°), a variation that indicates significant flexibility in the bonding of the thiolates to the Cu(I) ions.

Spectroscopy on Disulfido Complexes. (a) Absorption. The disulfido complexes **2a**−**j** are deeply colored because of multiple low-energy features in their absorption spectra. Plots of the spectra are presented in Figure S8 for those complexes that could be isolated analytically pure in bulk; the data for **2f** and **2g** are presented for illustrative purposes in Figure 7a. In general, similar spectral features are observed for all the complexes, which we assign by reference to the detailed analysis published for **2** (L = Tp^{iPr2}).[22] The spectrum of **2** (L = Tp^{iPr2}) contains two intense features at ∼28 000 ($\epsilon \approx 31\,200$ M^{-1} cm^{-1}) and ∼21 000 cm^{-1} ($\epsilon \approx 3700$ M^{-1} cm^{-1}) attributed to $\pi^* \rightarrow$ Cu(II) CT transitions originating from the $\pi^*_\sigma + xy + xy$ (hereafter designated as π^*_σ) and π^*_v orbitals, respectively (Figure 2). In addition, weaker d → d transitions at ∼15 000 ($\epsilon \approx 230$ M^{-1} cm^{-1}) and ∼10 300 cm^{-1} ($\epsilon \sim 130$ M^{-}1cm^{-1}) were reported. The spectra for complexes **2a**−**j** also exhibit intense bands between 20 000−28 000 cm^{-1}. In the case of the β-diketiminate complexes exemplified by **2f** and **2g** (Figure 7a), these are clearly resolved; for example, the maxima for **2g** are at ∼23 000 and ∼26 400 cm^{-1}. By analogy to the assignments for **2** (L = Tp^{iPr2}), the features are assigned as the out-of-plane

(30) On the basis of ^{1}H NMR spectroscopy, the Cu(I) complexes of ligands **a** and **h** lack a CH_3CN coligand.

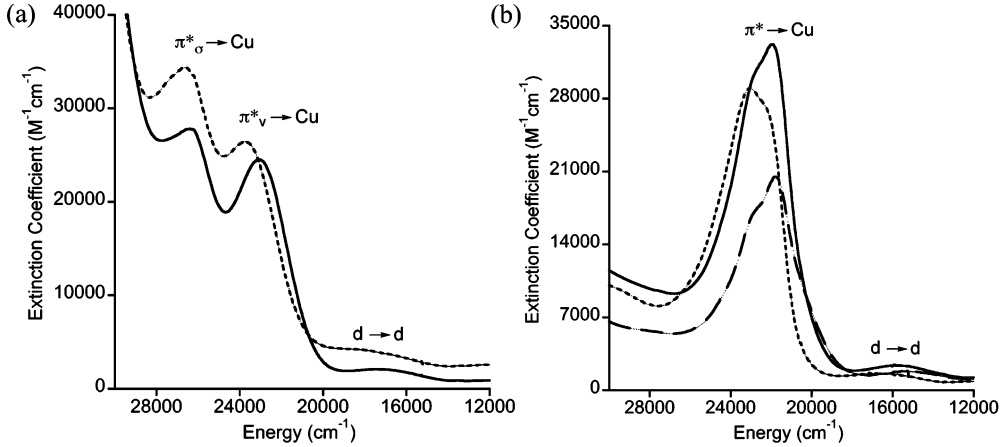

Figure 7. UV−vis absorption spectra of (a) β-diketiminate disulfido complexes **2f** (dashed line) and **2g** (solid line), and (b) anilido-imine disulfido complexes **2h** (long dashed line), **2i** (solid line), and **2j** (short dashed line). All spectra were measured in THF at ambient temperature. Proposed assignments are indicated (see text).

disulfide $\pi^*_v \rightarrow$ Cu(II) and the in-plane disulfide $\pi^*_\sigma \rightarrow$ Cu(II) CT transitions, respectively. The spectra also contain less intense features between 13 000−18 000 cm^{-1} that may be assigned as Cu d → d transitions. In general, the absorption features for the β-diketiminate complexes occur at higher energy than those of **2** (L = Tp^{iPr2}). Thus, the lower energy $\pi^*_v \rightarrow$ Cu(II) CT has a maximum at an energy of >23 000 cm^{-1} for **2a**−**g**, which is ≥2000 cm^{-1} greater than that of the corresponding feature at ∼21 000 cm^{-1} for **2** (L = Tp^{iPr2}). Similarly, the d → d transitions for the β-diketiminate compounds appear ∼1000−2000 cm^{-1} higher in energy than the ∼15 000 cm^{-1} band for **2** (L = Tp^{iPr2}). These discrepancies may be traced to differences in the strength of the Cu−S bonding, as described below (Discussion). Such Cu−S bonding differences also are likely to be the cause of more subtle variation of absorption spectral features seen when data for complexes with similar supporting ligands are compared. For example, the disulfide π^* → Cu(II) CT and d → d bands for **2f** are shifted to higher energy relative to **2g** (Figure 7a).

The absorption spectra for the anilido-imine disulfido complexes **2h**−**j** (Figure 7b) are unique, insofar as their π^* → Cu(II) CT bands appear to overlap and to lie at lower energy than the β-diketiminate analogs. The d → d features also are shifted to lower energy. Proper assignments of these spectra and rationales for their differences await more complete spectroscopic studies, which have yet to be performed.

(b) Resonance Raman. Using an excitation wavelength of 457.9 nm that falls within the $\pi^*_v \rightarrow$ Cu(II) CT transition, we obtained resonance Raman spectra of complexes **2a**−**j** prepared with $^{32}S_8$ or $^{34}S_8$. The spectra encompassing the region where sulfur-isotope-sensitive features were observed (300−550 cm^{-1}) are provided as Figures S9−S18; for illustration, the spectrum for **2d** is shown in Figure 8. All the spectra contain a sharp sulfur-isotope-sensitive peak ($\Delta\nu$-(^{34}S) = 8−13 cm^{-1}) that on the basis of precedent[22] is assigned to a predominantly ν(S−S) vibrational mode. The peak positions and isotope shifts are listed in Table 2. The ν(S−S) values for **2a**−**j** fall within a narrow range (424−454 cm^{-1}) notably lower than ν(S−S) = 500 cm^{-1} reported for **2** (L = Tp^{iPr2}). This latter value is similar to those reported for a wide range of disulfido complexes of transition metals (Table S2). Thus, the data indicate an especially high degree of S−S bond activation for the series of compounds **2a**−**j**.

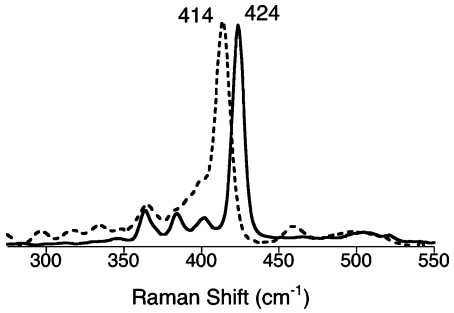

Figure 8. Resonance Raman spectra (λ_{ex} = 457.9 nm ≃ 21 900 cm^{-1}) of frozen benzene solutions (77 K) of $[Ph(H_2L^{Et2})Cu]_2(S_2)$ (**2d**, solid line for ^{32}S, dashed line for ^{34}S).

Scheme 2. Reactions of **2h** (L = HL'^{Me2}, **h**)

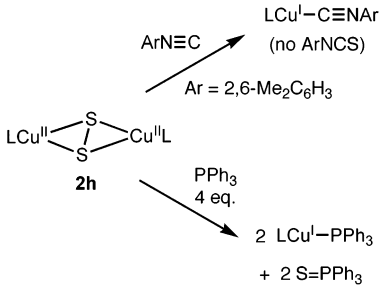

Reactivity. For the purposes of drawing some preliminary comparisons to the reactivity reported for **2** (L = Me_2-NPY2),[18] reactions of one of the disulfido complexes (**2h**) with PPh_3 and xylyl isocyanide were explored (Scheme 2). Monitoring by ^1H and ^{31}P NMR spectroscopy showed that, as seen for **2** (L = Me_2NPY2),[18] treatment of **2h** with 4 equiv of PPh_3 yielded 2 equiv of S=PPh_3 and 2 equiv of the Cu(I)−phosphine adduct (HL'^{Me2})Cu(PPh_3). This complex was identified on the basis of comparison to other known examples with β-diketiminate supporting ligands,[31] as well as by independent synthesis from (HL'^{Me2})Cu(CH_3CN). A

(31) Reynolds, A. M.; Lewis, E. L.; Aboelella, N. W.; Tolman, W. B. *Chem. Commun.* **2005**, 2014−2016.

similar reaction of **2h** with 2 equiv of PPh_3 resulted in incomplete conversion to 1 equiv of the phosphine adduct and 1 equiv of S═PPh_3, with half of **2h** remaining. This suggests similar efficiency for S-atom transfer to PPh_3 and trapping of Cu(I) by PPh_3, which differs from the results reported for **2** (L = Me_2NPY2), where 2 equiv of PPh_3 were reported to yield 2 equiv of S═PPh_3.[18,32]

The reactions of **2h** with xylyl isocyanide, O_2, and CO also proceeded differently than the same reactions with **2** (L = Me_2NPY2). While S-atom transfer was reported for reaction of **2** (L = Me_2NPY2) with xylyl isocyanide to yield ArN═C═S,[18] we observed clean conversion of **2h** to the Cu(I) adduct of the unfunctionalized isocyanide, (HL'^{Me2})-Cu(CNAr) (no effort to determine the fate of the S_2^{2-} fragment was made). This complex was identified by comparison to other examples,[45] as well as by independent synthesis. Complex **2h** was unreactive with O_2 (1 atm, ~1 h, room temperature, THF, UV−vis) or CO (1 atm, 20 min, room temperature, C_6D_6, NMR), in contrast to **2** (L = Me_2-NPY2), which yielded peroxodicopper and Cu(I)−CO complexes, respectively.[18]

Discussion

The reaction of S_8 with Cu(I) complexes of a series of anionic, bidentate N-donor ligands (Figure 3) yielded a series of (μ-η^2:η^2-disulfido)dicopper complexes **2a**−**j**. In the case of the β-diketiminate ligands, in particular those that contain an unsubstituted methine position (**a**−**c**), the syntheses are complicated by further reaction to yield the clusters **5**, which were isolated for ligands **a** and **b**. A related sensitivity of β-diketiminate ligands toward reaction at the methine position has been reported previously.[33] The ligand functionalization is avoided entirely when anilido-imine ligands **h**−**j** are used. X-ray structures of **5a** and **5b** reveal that, despite their different alkyl substituents, they are conformational isomers. Their cyclic $Cu_4(SR)_4$ topologies differ with respect to their Cu−Cu distances and Cu−S−Cu angles, such that **5b** is puckered relative to **5a**.

A primary goal of this work is to assess the structural and spectroscopic properties of the disulfido complexes **2a**−**j** to understand supporting ligand effects on S−S bond activation. The relevant experimental data are best understood by recourse to the bonding picture for the $[Cu_2(\mu\text{-}\eta^2\text{:}\eta^2\text{-}S_2)]^{2+}$ core (and peroxo analogs) shown in Figure 2.[22] According to this picture, increased Cu−S bonding interactions results in greater backbonding from the filled Cu d_{xy} orbitals into the empty S_2^{2-} σ* orbital and a lowering of the S−S bond order (i.e., greater S−S bond activation). Stronger bonding interactions between the Cu ions and the disulfide fragment also cause an increase in the energy splitting of the frontier orbitals, notably a lowering of the $\pi^*_\sigma + d_{xy} + d_{xy}$ and the HOMO concomitant with a raising of the LUMO ($\pi^*_\sigma + d_{xy} - d_{xy}$). Experimentally, these shifts are indicated by increases in the energies of the $\pi^*_v \rightarrow$ Cu(II) and $\pi^*_\sigma \rightarrow$ Cu(II) CT transitions in absorption spectra.[22] In addition, X-ray crystallographic and vibrational spectroscopic data enable the extent of Cu−S bond strengthening and S−S bond weakening to be directly discerned. Observation of appropriate correlations among the experimental parameters provides support for the bonding picture and enables the specific role of ligand structural variation on S−S bond activation to be determined.

The X-ray structural and resonance Raman data show that the degree of S−S bond activation in the $[Cu_2(\mu\text{-}\eta^2\text{:}\eta^2\text{-}S_2)]^{2+}$ complexes of bidentate, anionic β-diketiminate and anilido-imine ligands is generally greater than in other disulfido complexes of copper and other transition metals. As illustrated in Figure 5 (Table 2), with one exception (**2c**), the complexes **2a**−**j** feature shorter Cu−S, longer Cu−Cu, and longer S−S distances than **2** (L = ii or Me_2NPY2). The correlated trends are consistent with the bonding picture in Figure 2; shorter Cu−S distances indicate stronger Cu−S bonds, which result in shorter Cu−Cu distances and a lowering of the S−S bond order (longer S−S distance) through greater backbonding into the S_2^{2-} σ* orbital. Complexes **2c**, **2j**, and **2** (L = Tp^{iPr2} or Me_2NPY2), which exhibit Cu−S > 2.21 Å, Cu−Cu > 3.85 Å, and S−S < 2.17 Å, are at one extreme in Figure 5. Notably, the S−S distance in **2** (L = Tp^{iPr2}) of 2.073(4) Å is close to that of H_2S_2 (2.055 Å), both of which fall within the range of values reported for a large sampling of transition metal disulfido complexes (~2.00−2.08 Å, Table S2).[34] Complexes **2a**, **d**, and **h** are at the other extreme, with Cu−S < 2.195 Å, Cu−Cu < 3.79 Å, and S−S > 2.21 Å values that are indicative of an extraordinary degree of S−S bond activation. Indeed, a search of the CSD[35] revealed only a few examples of complexes with S_2^{2-} ligands featuring S−S bond distances of >2.2 Å. The S_2^{2-} ligand is bound to three or more metal ions in several of these,[36] leaving three cases with μ-η^2:η^2-disulfido moieties bridging two Ni (S−S = 2.298 and 2.209 Å)[37] or Re ions (S−S = 2.228 Å).[38]

The generally high degree of S−S bond activation in **2a-j** is further supported by the resonance Raman spectra, which feature peaks attributed to predominantly ν(S−S) modes on the basis of their positions and ^{34}S-isotope shifts. The peak positions for **2a**−**j** are >45 cm^{-1} lower than that of **1** or **2**

(32) Trapping of released sulfur (e.g., as S_8) by free PPh_3 is a possible pathway,[32a] which only further mechanistic studies can validate or refute. Bartlett, P. D.; Meguerian, G. *J. Am. Chem. Soc.* **1956**, *78*, 3710−3715.

(33) (a) Yokota, S.; Tachi, Y.; Itoh, S. *Inorg. Chem.* **2002**, *41*, 1342−1344. (b) Jazdzewski, B. A.; Holland, P. L.; Pink, M.; Young, V. G., Jr.; Spencer, D. J. E.; Tolman, W. B. *Inorg. Chem.* **2001**, *40*, 6097−6107. (c) Radzewich, C. E.; Coles, M. P.; Jordan, R. F. *J. Am. Chem. Soc.* **1998**, *120*, 9384−9385. (d) Fekl, U.; Kaminsky, W.; Goldberg, K. I. *J. Am. Chem. Soc.* **2001**, *123*, 6423−6424.

(34) Müller, A.; Jaegermann, W.; Enemark, J. H. *Coord. Chem. Rev.* **1982**, *46*, 245−280.

(35) Cambridge Structure Database, version 5.27, November 2005.

(36) (a) $Cp_2Ni_2Mn_4(CO)_{14}(\mu_6\text{-}S_2)(\mu_3\text{-}S)_2$, S−S = 2.2573(12) Å. Adams, R. D.; Miao, S.; Smith, M. D.; Farach, H.; Webster, C. E.; Manson, J.; Hall, M. B. *Inorg. Chem.* **2004**, *43*, 2515−2525. (b) $[(Cp^*Ru)_3(\mu_3\text{-}S_2)(\mu_3\text{-}S)(\mu_2\text{-}SEt)]^{2+}$, S−S = 2.210(3) Å. Houser, E. J.; Krautscheid, H.; Rauchfuss, T. B.; Wilson, S. R. *Chem. Commun.* **1994**, 1283−1284.

(37) (a) Pleus, R. J.; Waden, H.; Saak, W.; Haase, D.; Pohl, S. *J. Chem. Soc., Dalton Trans.* **1999**, 2601−2610. (b) Mealli, C.; Midollini, S. *Inorg. Chem.* **1983**, *22*, 2785−2786.

(38) Rakowski DuBois, M.; Jagirdar, B. R.; Dietz, S.; Noll, B. C. *Organometallics* **1997**, *16*, 294−296.

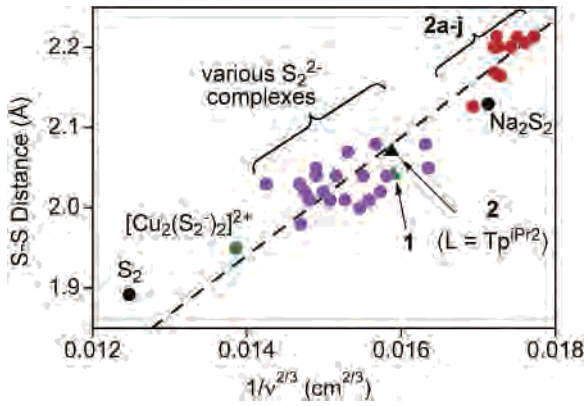

Figure 9. Plot of the S−S distance (Å) versus $1/\nu^{2/3}$ ($cm^{2/3}$), where ν = S−S vibrational mode. The various S_2^{2-} complexes shown as purple circles are listed in Table S2. The dashed line is a linear least-squares fit of the data to eq 1, with slope = C_{S-S} = 63.95 and intercept = $d_{S=S}$ = 1.063 (R = 0.93).

(L = Tp^{iPr2}), consistent with lower S−S bond orders for the former class. The data may be further analyzed by application of Badger's Rule (eq 1), an empirical relationship

$$r_e = \frac{C_{ij}}{\nu_e^{2/3}} + d_{ij} \qquad (1)$$

between an equilibrium bond distance (r_e) and its associated stretching frequency (ν_e) in a series of related species.[39] Usually applied to small polyatomic molecules, it has also recently been found to be useful for assessing heme and nonheme iron−oxygen bonds.[40] A plot of S−S distance versus $1/\nu^{2/3}$ is shown in Figure 9 for **2a**−**j** (red circles), **2** (L = Tp^{iPr2}) (black triangles), **1** (green triangles), and a large sampling from the large class of known transition metal disulfido complexes (purple circles, listed in Table S2). Also shown are data for Na_2S_2 and S_2,[41] taken as representative of S−S single and S═S double bonds, respectively (black circles). Further perspective is provided by a data point (green circle) corresponding to the μ-1,2-disulfido(·1−) moiety in a recently reported dicopper complex.[13c] The data fit reasonably well to eq 1 with parameters C = 63.95 and d = 1.063 (dashed line, R = 0.93), although the scatter about the line is greater than that reported for a similar plot of Fe−O bonds in heme species over similar ranges of distances ($\Delta \approx 0.3$ Å) and stretching frequencies ($\Delta \approx 300-350$ cm^{-1}).[40] We speculate that this may be caused by the ν(S−S) features not always being pure S−S stretches, a notion supported by calculations reported for **2** (L = Tp^{iPr2}) that indicate that its 500 cm^{-1} mode has 63% S−S and 37% Cu−S character.[22] With this caveat in mind, a number of broad conclusions can nonetheless be drawn from the linear correlation in Figure 9. Although tightly clustered, the data for **2a**−**j** lie at one extreme, indicative of S−S bond orders even smaller than that in Na_2S_2 (bond order formally equal to one, but with an S−S bond considered to be slightly elongated because of lone pair-lone pair repulsions). Complexes **1** and **2** (L = Tp^{iPr2}) fall within the regime of the sampling of typical transition metal disulfido complexes (purple circles, bond order formally equal to 1). These generally feature weaker S−S bonds than that of S_2^- (green circle, bond order ≈1.5) and S_2 (bond order = 2).

The weak S−S bonds in **2a-j** may be attributed to the presence of the strongly electron-donating β-diketiminate and anilido-imine supporting ligands, which are effective at inducing back-donation from the copper ions into the S−S σ* orbital. Accordingly, this effect is decreased in **2** (L = Tp^{iPr2} or Me_2NPY2) because the supporting ligands are poorer electron donors, resulting in shorter and stronger S−S bonds. The differences in the electron-donating capabilities of the supporting ligands are also manifested in differences in the Cu−S bonding, as revealed experimentally by the energies of the $\pi \rightarrow$ Cu(II) CT and d $\rightarrow$ d transitions in electronic absorption spectra. These transition energies are generally higher in **2a**−**j** than in **2** (L = Tp^{iPr2} or Me_2NPY2), reflecting greater splitting of the frontier molecular orbitals and stronger Cu−S bonding (Figure 2).

The relative electron-donating power of β-diketiminate/anilido-imine versus tris(pyrazolyl)hydroborate ligands was identified previously as a key determinant of the electronic structures of 1:1 Cu/O_2 adducts (peroxo-Cu(III) vs superoxo-Cu(II))[42] and Cu−thiolate models of type 1 copper electron-transfer sites.[43] Differences in the relative stability of bis(μ-oxo)- versus μ-η^2:η^2-peroxodicopper isomers have also been linked to the electron-donating capabilities of these supporting ligands.[44] A finding of particular significance here is the sole observation of bis(μ-oxo)dicopper complexes with the β-diketiminate ligands **a**, **b**, **d**−**g** (which stabilize the formal Cu(III) state).[45] In contrast, analogous bis(μ-sulfido)dicopper(III) cores appear not to be accessible, which has been verified by theoretical calculations.[13a] Despite the S−S bond weakening evident in **2a**−**j**, the lower electronegativity of sulfur relative to oxygen renders cleavage of the S−S bond in the disulfidodicopper core less favorable than that of the O−O bond in the peroxodicopper congener.

Differences in the degree of S−S bond activation within the series **2a**−**j** are most clearly evident from the bond distances (Figure 5)[46] and can generally be attributed to steric effects. For those ligands with relatively small aryl substituents (R″ = Me or Et; **a**, **b**, **d**, **f**, **h**) or with larger ^{i}Pr groups but which feature R′ = H (thus allowing the aryl group to

(39) Badger, R. M. *J. Chem. Phys.* **1935**, *3*, 710−714.
(40) Green, M. T. *J. Am. Chem. Soc.* **2006**, *128*, 1902−1906.
(41) Müller, A.; Jaegermann, W. *Inorg. Chem.* **1979**, *18*, 2631−2633.
(42) (a) Cramer, C. J.; Tolman, W. B.; Theopold, K. H.; Rheingold, A. L. *Proc. Natl. Acad. Sci. U.S.A.* **2003**, *100*, 3635−3640. (b) Aboelella, N. W.; Kryatov, S. V.; Gherman, B. F.; Brennessel, W. W.; Young, V. G., Jr.; Sarangi, R.; Rybak-Akimova, E. V.; Hodgson, K. O.; Hedman, B.; Solomon, E. I.; Cramer, C. J.; Tolman, W. B. *J. Am. Chem. Soc.* **2004**, *126*, 16896−16911. (c) Sarangi, R.; Aboelella, N.; Fujisawa, K.; Tolman, W. B.; Hedman, B.; Hodgson, K. O.; Solomon, E. I. *J. Am. Chem. Soc.* **2006**, *128*, 8286−8296.
(43) Randall, D. W.; DeBeer, S.; Holland, P. L.; Hedman, B.; Hodgson, K. O.; Tolman, W. B.; Solomon, E. I. *J. Am. Chem. Soc.* **2000**, *122*, 11632−11648.
(44) Mirica, L. M.; Ottenwaelder, X.; Stack, T. D. P. *Chem. Rev.* **2004**, *104*, 1013−1045.
(45) Spencer, D. J. E.; Reynolds, A. M.; Holland, P. L.; Jazdzewski, B. A.; Duboc-Toia, C.; Pape, L. L.; Yokota, S.; Tachi, Y.; Itoh, S.; Tolman, W. B. *Inorg. Chem.* **2002**, *41*, 6307−6321.
(46) A clear trend in ν(S−S) values for **2a**−**j** is less obvious, perhaps also because these vibrational modes are not pure S-S stretches.

'bend back'; **e**, **g**, **i**), the full electronic donor influence of the ligands is manifested by longer S−S, shorter Cu−S, and shorter Cu−Cu distances. The ligands **c** and **j** are significantly more sterically congested because of the presence of ^{i}Pr aryl (R″) substituents and Me or tBu backbone (R′) groups.[47] We postulate that this congestion is the underlying cause of the relatively longer Cu−S and Cu−Cu distances and the decreased level of S−S bond activation in their disulfido complexes. These steric effects for **c** and **j** have precedent in Cu/O_2 chemistry, since reactions of O_2 with Cu(I) complexes of these ligands yield 1:1 adducts[42b,48] instead of bis(μ-oxo) complexes seen with **a**, **b**, and **d**−**g**.[45]

Preliminary investigation of the reactivity of one of the disulfido complexes (**2h**) showed some similarity to that previously reported for **2** (L = Me_2NPY2),[18] although significant differences also were seen (Scheme 2). Thus, S-atom transfer to PPh_3 with trapping of the resulting Cu(I) sites by excess phosphine was observed for both, but the results with only 2 equiv of PPh_3 differed. For **2** (L = Me_2NPY2), complete S-atom transfer to yield 2 equiv of S=PPh_3 was reported,[18] but we found that **2h** yielded 1 equiv of S=PPh_3 and 1 equiv of the Cu(I)−phosphine adduct, with half of **2h** left unreacted. These results imply that S-atom transfer from **2** (L = Me_2NPY2) outpaces trapping of the Cu(I) complex by PPh_3, wheareas for **2h** the two processes are more closely competitive. Poorer S-atom transfer capabilities for **2h** relative to **2** (L = Me_2NPY2) are also suggested by the results of reactions with xylyl isocyanide, which for the former gave the Cu(I) adduct of the isocyanide, but for the latter yielded the product of S-atom incorporation, ArN=C=S. In addition, the lack of reactivity of **2h** with O_2 and CO contrasts with reactions of these reagents with **2** (L = Me_2NPY2), which yielded peroxodicopper or Cu(I)−CO species, respectively.

Conclusions

Through the synthesis and detailed structural and spectroscopic characterization of the series of complexes **2a**−**j** that feature the $[Cu_2(\mu\text{-}\eta^2\text{:}\eta^2\text{-}S_2)]^{2+}$ core, the degree of S−S bond activation as a function of supporting ligand was assessed. In general, the strong electron donating power of the β-diketiminate and related anilido-imine ligands results in strong Cu−S interactions that are correlated with weak S−S bonds and short Cu−Cu distances. In addition to the structural correlation of the Cu−S, S−S, and Cu−Cu distances within the $[Cu_2(\mu\text{-}\eta^2\text{:}\eta^2\text{-}S_2)]^{2+}$ core (Figure 5), the S−S distances also correlate inversely with the ν(S−S) value measured by resonance Raman spectroscopy (Badger's rule, Figure 9). A comparison to a range of other species that feature S_2^{n-} units places **2a**−**j** at the extreme of weak S−S bonding (long S−S and low ν(S−S)) that corresponds to particularly powerful S−S bond activation. These phenomena, as well as the observation of increased energies for $\pi \rightarrow$ Cu(II) CT and d → d transitions in electronic absorption spectra, may be understood in terms of a previously proposed bonding picture (Figure 2). According to this picture, large frontier orbital energy splittings result from strong Cu−S bonding, with the powerful electron-donating capabilities of the β-diketiminate and anilido-imine ligands underlying increased backbonding into the S_2^{2-} σ* orbital, which weakens the S−S bond. These ligand effects are mitigated by steric hindrance provided by bulky substituents, which yield complexes with longer Cu−Cu and shorter S−S distances.

The $[Cu_2(\mu\text{-}\eta^2\text{:}\eta^2\text{-}S_2)]^{2+}$ complexes supported by β-diketiminate or anilido-imine ligands also exhibit unique reactivity. Sulfur transfer to the central methine carbon of the β-diketiminate ligands yields $[Cu(SR)]_4$ clusters **5**, which may adopt different conformations depending on the ligand substituents. This reaction is prevented when the anilido-imine ligands are used (**2h**−**j**). A preliminary reactivity study of **2h** revealed facile sulfur transfer to added PPh_3, but only displacement without sulfur insertion upon reaction with xylyl isocyanide, and no reactions with O_2 or CO. In comparison to **2** (L = Me_2NPY2), the sulfur moiety in **2h** appears to be less reactive, with trapping of the copper ions to yield Cu(I)−X (X = PPh_3 or ArNC) complexes being more facile.

Acknowledgment. We thank the NIH for financial support of this research (GM47365 to W.B.T. and GM68307 to E.C.B.) and Dr. Lyndal Hill for assistance with data analysis and preparation of Figure 5.

Supporting Information Available: Crystallographic data in CIF format, experimental information for (HL′^{Me2})Cu, tables showing a summary of the crystallographic data and the S-S bond lengths and vibrational frequencies, and figures showing the X-ray crystal structure of **2a**, **c**, **e**−**h**, and **j**, the electronic absorption spectra the the disulfido dicopper complexes, and the resonance Raman spectra of **2a**−**j**. This material is available free of charge via the Internet at http://pubs.acs.org.

IC061589R

(47) Smith, J. M.; Lachicotte, R. J.; Holland, P. L. *Chem. Commun.* **2001**, 1542−1543.

(48) (a) Aboelella, N. W.; Lewis, E. A.; Reynolds, A. M.; Brennessel, W. W.; Cramer, C. J.; Tolman, W. B. *J. Am. Chem. Soc.* **2002**, *124*, 10660−10661. (b) Reynolds, A. M.; Gherman, B. F.; Cramer, C. J.; Tolman, W. B. *Inorg. Chem.* **2005**, *44*, 6989−6997.